Development of a numerical wind atlas for South Africa

Lennard, Christopher ; Hahmann, Andrea N.; Badger, Jake; Mortensen, Niels Gylling; Argent, Brendan

Published in:
Energy Procedia

Link to article, DOI:
10.1016/j.egypro.2015.07.873

Publication date:
2015

Document Version
Publisher's PDF, also known as Version of record

Available online at www.sciencedirect.com

ScienceDirect

Energy Procedia 76 (2015) 128 – 137

Energy Procedia

European Geosciences Union General Assembly 2015, EGU

Division Energy, Resources & Environment, ERE

Development of a numerical wind atlas for South Africa

Christopher Lennard[a]*, Andrea N. Hahmann[b], Jake Badger[b], Niels G. Mortensen[b], Brendan Argent[a]

[a]*Climate Systems Analysis Group, University of Cape Town, Rondebosch, Cape Town, 7945, South Africa*
[b]*Department of Wind Energy, Technical University of Denmark, Roskilde, 4000, Denmark*

Abstract

Two verified wind atlases have been developed for South Africa. The first adopted a statistical-dynamical approach and the second a novel, fully dynamical approach. We verify the atlases against an observational wind atlas generated from three years of data from 10 measurement masts. The statistical-dynamical method underestimates the generalized mean wind speeds at the observation sites whereas the fully dynamical method has lower biases and slightly overestimates the generalized mean wind speeds. The dynamical method captures thermally forced dynamical processes and also resolves topographically enhanced flows the statistical-dynamical method cannot.

Peer-review under responsibility of the GFZ German Research Centre for Geosciences

Keywords: Numerical wind atlas; South Africa; KAMM; WRF; WAsP; wind atlas methodology

1. Introduction

The assessment of wind resource in regions where measurements are sparse usually involves the calculation of a generalized wind climate from observations and models to give an indication of the geographical distribution of wind resource for feasibility studies and decision-making processes. A number of methods are available to construct regional or global wind climates and include simple folklore, measurements only, measure-correlate-predict,

* Corresponding author. Tel.: +27-21-650-2684; fax: +27-21-650-5773.
E-mail address: lennard@csag.uct.ac.za

Peer-review under responsibility of the GFZ German Research Centre for Geosciences
doi:10.1016/j.egypro.2015.07.873

reanalysis data, and mesoscale modelling [1]. The observation-based wind atlas (OWA) method has become a commonly used method in which microscale modelling produces a generalized regional wind climate based on some input data. The generalized wind climate of a region is an idealized wind climate that would exist if the surface had no obstacles, was flat, had uniform roughness and were subject to the same atmospheric conditions as the measuring position [1].

In regions with poor observational coverage, the OWA method and some form of mesoscale modelling can be combined. One such method uses the Karlsruhe Atmospheric Mesoscale Model (KAMM) [2] and the Wind Atlas Analysis and Application Programme (WAsP) microscale model, more commonly known as the KAMM-WAsP wind atlas method. This method is fully described in [3] and has been validated [4,5] and used to develop wind atlases in a number of regions, e.g. Europe [6,7], Egypt [8] and Finland [9]. More recently, this method has been extended to use the output from the Weather, Research and Forecasting (WRF [10]) Model [11,12].

The Wind Atlas for South Africa project (WASA) has produced two verified wind atlases for parts of South Africa using these two methods. An extensive description of the methods and results are available from [12]. The KAMM-WAsP method is based on a statistical-dynamical way of running the mesoscale model and combining the results, whereas the WRF-WAsP method uses WRF in a fully dynamical mode (see section 1.2). The two methods produced what is called Numerical Wind Atlases (NWA). The WASA project includes a measurement campaign that erected 10 masts with instruments at four levels; the data from which the observational wind atlas (OWA) was developed. A complete description is presented in [13,14].

The OWA results can be compared to generalized wind climates derived from the KAMM- and WRF-based NWA to assess the different mesoscale model methods in a wind energy context – as wind energy is a function of the cube of the wind speed, small differences in wind speeds may have large consequence for energy assessment e.g. a 5% difference in wind speed means up to a 15% difference in kinetic energy flux. The actual energy assessment depends on the wind turbine and its power curve.

This paper presents the two mesoscale model methods and subsequent microscale results to quantify the error of each and wind energy assessment implications.

2. Mesoscale methods

2.1. KAMM

This methodology adopts a statistical-dynamical downscaling approach [15] that assumes a robust relationship between meteorological situations at the large-scale and meteorological situations at the small-scale. The NCEP2 reanalysis data [16] between 1980 and 2009 are used as the large-scale field from which a number of wind classes (large-scale wind circulation states) are developed for three domains over South Africa (Fig. 1). Each of the wind classes (Fig. 2) is downscaled using the mesoscale model KAMM to capture regional scale topographic modification of the wind field. Post-processing of the results from all the simulations yields a wind resource map at the resolution of the model (5 km) at any chosen height above ground level, as well as a generalized [3] wind climate map or numerical wind atlas.

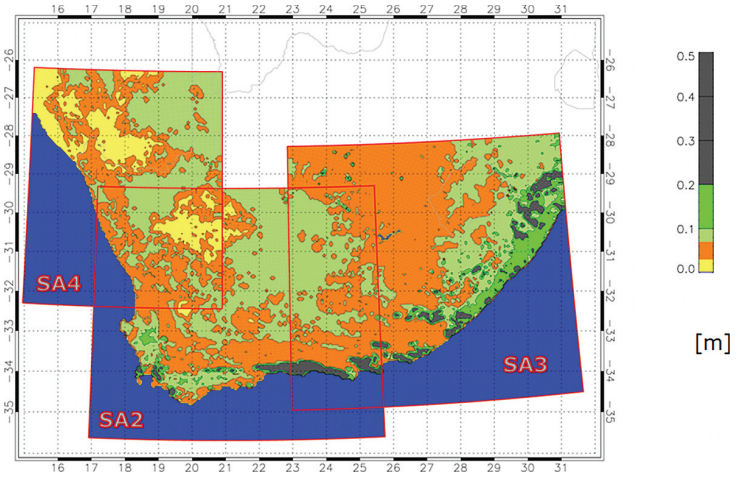

Fig. 1. The surface aerodynamic roughness length for the three modelling domains at a resolution of 5 km. The domain boundaries are marked by red lines, and labeled SA2, SA3, SA4. The colour key is given on the right hand side. The roughness data is derived from the United States Geological Survey (USGS) Global Land Cover Classification (GLCC).

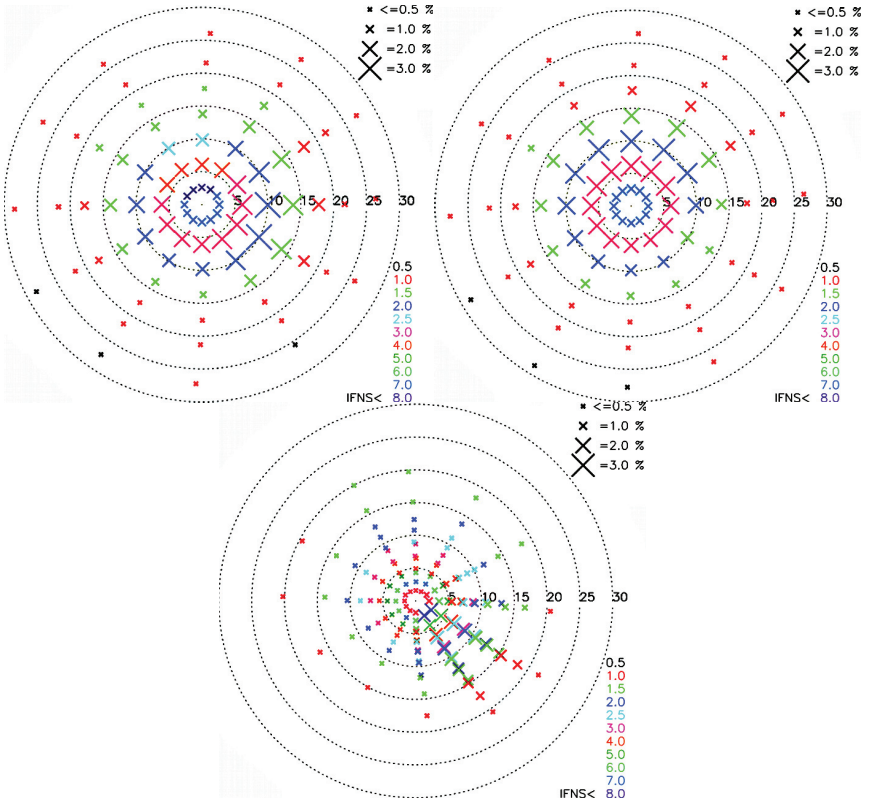

Fig. 2. The geostrophic wind classes for SA2 (top left – 84 classes), SA3 (top right – 84 classes) and SA4 (bottom – 137 classes) domains based on NCEP2 reanalysis data over the period 1980–2009. Each cross represents a forcing wind speed (distance from the centre of the diagram) and direction. The speed scale is in ms^{-1}. The size of each cross represents the probability of the wind class. The frequency scale is given in the upper right hand corner. The color scale indicating the inverse Froude number squared (IFNS) is given in the lower right hand corner.

2.2. WRF

The WRF model is a mesoscale numerical weather prediction system designed to serve both operational forecasting and atmospheric research. It is non-hydrostatic and adopts a nested domain strategy in which consecutively high-resolution domains are nested in coarser-resolution domains. It is highly configurable having a number sub-grid scale parameterizations, including many of the boundary layer that are critical for wind energy applications.

The WASA numerical wind atlas utilized the Advanced Research WRF (ARW-WRF) version 3.5.1. The simulation used 3 domains with horizontal resolutions of 27 km, 9 km and 3 km respectively (Fig. 3). In the vertical, the model was configured with 41 levels with model top at 50 hPa. The lowest 12 of these levels are within 1000 m of the surface and the first level is located at approximately 14 m above ground level (AGL). The 6-hourly ERA-Interim reanalysis [17] provided initial and boundary conditions and the simulation spanned October 2009 to September 2013.

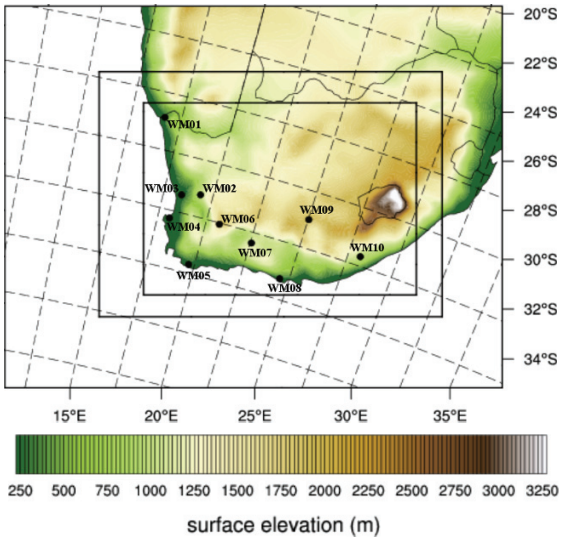

Fig. 3. Configuration of the WRF model domains and terrain elevation (m). The inner lines show the position of the 9 km and 3 km domain, respectively. The locations of the WASA masts are shown by the dots.

Sensitivity tests were carried out to determine the optimal model configuration using the OWA for the evaluation. The only large sensitivity found was the choice of land surface scheme, both because of the land surface model itself and also because of the different treatment of the surface roughness length. Besides this, once a domain configuration and horizontal grid spacing is selected, there is very little sensitivity to most physics options with respect to the annual mean wind speed at 100 m AGL.

The final model configuration used the Kain-Fritch convective parameterization (except in the 3 km domain where convection is explicitly resolved), Mellor-Yamada-Janjic land-surface and planetary boundary layer scheme, the Noah Land Surface Model and the NOAA/NCEP ~10×10 km resolution daily sea surface temperatures [18]. For wind energy applications, the use of a constant surface roughness length is necessary to remain consistent with the generalization procedure, so the annual cycle available in the WRF model was disabled and the winter (shorter) length used throughout the simulation period.

In the 27 km and 9 km domains (domains 1 and 2) data were output every 3 hours and in domain 3, every hour. Additionally, in the lowest 7 levels of domain 3, wind speed data were output every 10 minutes. The model wind components were interpolated to the coordinates of the mass grid and then used to compute the wind speed and rotated to the true north to derive the wind direction. In the vertical, for a given height, e.g., 100 m, wind speeds are interpolated between neighboring model levels using logarithmic interpolation in height.

A new procedure was developed to process the WRF-based wind climate [12] so that a proper verification of wind climate estimates derived from mesoscale modeling could be carried out. Without this step verification is not possible because the land surface description within the model does not agree with reality, and therefore model winds will not agree with measured winds.

To summarize, in the KAMM-WAsP method the mesoscale model is run to obtain a single state for each of the wind classes derived from the NCEP2 data whereas in the WRF-based method the mesoscale model simulates a time continuous period overlapping with the observation record, and outputs data at corresponding time steps. In the KAMM the lower boundary has uniform land temperature (relative to initial air temperature) and sea surface temperature whereas in the WRF model simulations the lower boundary has an interactive land surface and time varying sea surface temperature (Table 1).

The generalized winds from both mesoscale methods were evaluated against the observational wind atlas to assess error at each measurement site. Additionally, data from each 3 km × 3 km WRF grid cell that had a measurement site situated in it were evaluated against the observed data to assess the simulated wind speed distribution and the diurnal and seasonal cycles.

Table 1. Fundamental differences between the KAMM and WRF-based NWA methods.

KAMM	WRF
"Steady state" simulation of each of the 307 wind classes.	Time-integrated simulation that provides a continuous time series for each grid cell
Each simulation is initialized with a single vertical representation of the atmosphere	Simulation is initialized with the 3-dimensional state of the atmosphere
Lower boundary condition has uniform land and sea surface temperature	Lower boundary has interactive land and time-varying sea surface temperatures

3. Evaluation results

3.1. KAMM vs. WRF

The long-term averaged generalized wind speed for the observations and the model simulations are compared using the NWA derived from KAMM and WRF with the OWA derived at all the WASA masts (Table 2). The generalized winds correspond to a height of 100 m AGL and a roughness length of 0.03 m. The observed mean wind speeds are derived from the measurements through microscale modelling. Most OWA values are for the period 1 October 2010 - 30 September 2013, except for WM04, WM08-WM10 that contain some missing data.

Table 2. Comparison of the mean generalized wind speed (h=100 m and z_0=0.03 m) for all WASA masts for the observations (U_{Obs}), and the NWA from KAMM (U_{KAMM}) and WRF (U_{WRF}). The KAMM-derived NWA values are for the period 1 October 2010 to 30 September 2013 for all sites. In the WRF-derived NWA values, the time period is 1 October 2010 to 30 September 2013 for most sites, but 1 June 2010 to 31 May 2013 for WM04; 1 March 2011 to 28 February 2012 and 1 October 2012 to 30 September 2013 for WM10. U_{Obs} has been derived using default (−40 Wm^{-2}) mean heat flux over land.

Station	U_{Obs} (ms^{-1})	U_{KAMM} (ms^{-1})	$U_{KAMM}-U_{Obs}$ (%)	U_{WRF} (ms^{-1})	$U_{WRF}-U_{Obs}$ (%)
WM01 Alexander Bay	6.83	5.53	−19.0	6.73	−1.5
WM02 Calvinia	6.68	7.03	5.2	7.31	9.4
WM03 Vredendal	7.38	6.70	−9.2	6.99	−5.3
WM04 Vredenburg	7.50	7.16	−4.5	8.15	8.7
WM05 Napier	8.98	8.59	−4.3	9.08	1.1
WM06 Sutherland	7.86	7.33	−6.7	8.27	5.2
WM07 Beaufort West	7.78	6.69	−14.0	7.39	−5.0
WM08 Humansdorp	8.01	7.61	−5.0	8.08	0.9
WM09 Noupoort	8.33	7.41	−11.0	8.45	1.4
WM10 Butterworth	7.12	6.14	−13.8	7.53	5.8
Mean Error			−8.2		2.1
Mean Absolute Error			9.3		4.4

The biases between generalized wind derived from OWA and NWA vary greatly with model and site. Overall, the KAMM-derived mean generalized winds are underestimated for most sites except for WM02. The sites where thermal-induced flows are important in determining the wind climate (e.g. WM01, WM03) are the most affected. In the WRF-derived NWA, biases are mostly positive, except for WM01, WM03, and WM07, but the absolute value of all biases is smaller than 10%. At two of the sites, WM02 and WM10, the bias is quite large, and probably attributable to overestimation of winds under stable conditions. The mean error metrics in the WRF-derived NWA are at least half those of the KAMM-derived atlas.

At each site the wind climate of the two NWAs are evaluated against the respective OWA. Selected examples are presented here that demonstrate the general results. At Alexander Bay (WM01), a site that experiences thermal wind forcing as a result of the pressure gradient between the hot desert and cold Benguela ocean current, the KAMM wind climate is over-dominated by southerly flow and the annual mean wind speed is greatly underestimated (Fig. 4, top row). The WRF wind climate shows very good agreement with both the observed wind rose and wind speed distribution between sectors. At Napier (WM05), a region that is largely dominated by synoptic processes, both atlases compare well with the OWA (Fig. 4, centre row). In a more mountainous region (Butterworth, WM10), there is no preferred wind sector in the OWA and the mean wind speed is relatively low (Fig. 4, bottom row). The KAMM atlas underestimates the wind speed climate here and does not capture the sector distribution well whereas the WRF atlas more correctly captures the sector distribution but slightly overestimates the wind speed climate.

The WRF-derived atlas is consistently more similar to the OWA than the KAMM atlas in terms of error and wind climate.

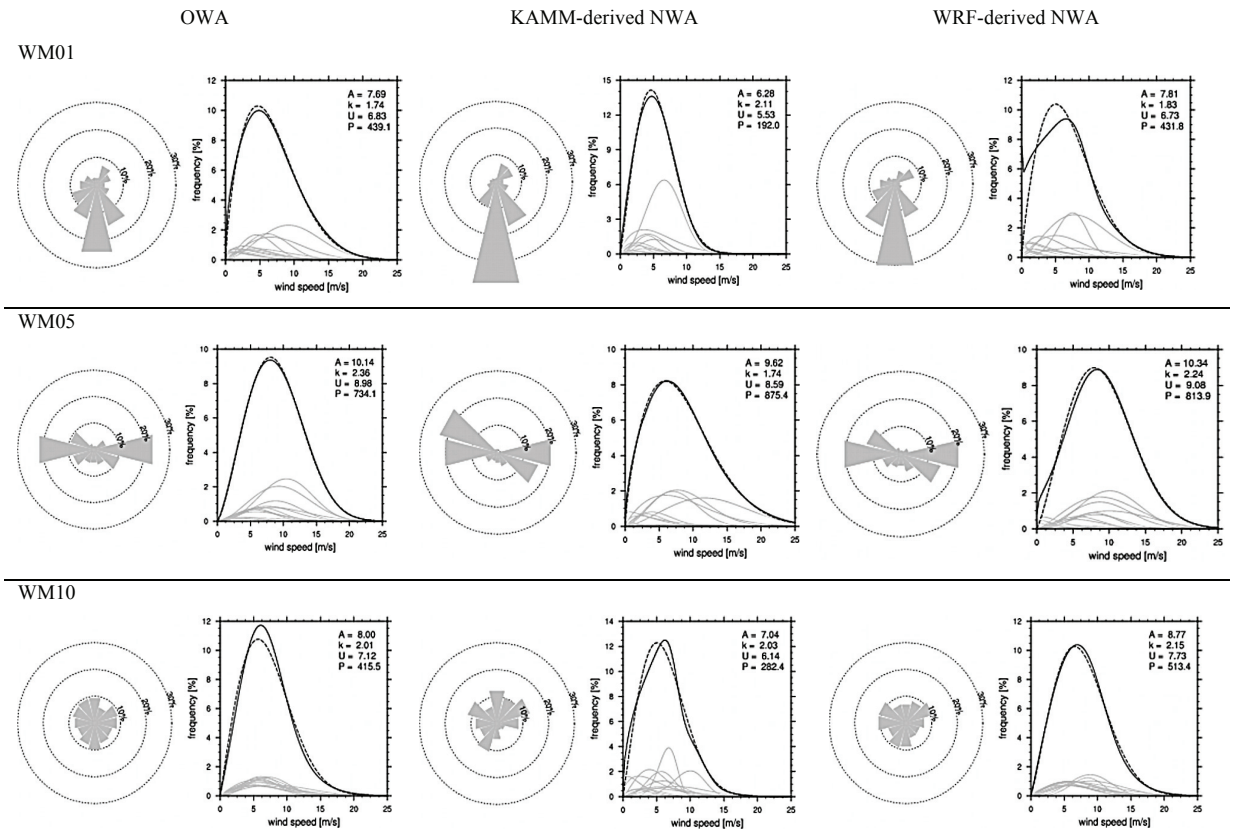

Fig. 4. Graphical representation of the WAsP generalized wind climate files as a wind rose at WM01 (top row), WM05 (centre row) and WM10 (bottom row). In each panel the wind rose on the left shows the frequency each wind sector is mapped to and on the right the wind speed distribution for each sector (grey lines) and the combined for all sectors (dark solid line is the emergent distribution and dashed line is the combined Weibull frequency distribution. The OWAs and NWAs are based on the period October 2010 to 30 September 2013 except at WM10 where the OWA is based on the periods 1 March 2011-February 2012 and October 2012-September 2013 as a result of vandalism at the site. In the top right corner of the wind speed distribution panel are the Weibull *A*- and *k*- parameters, the mean wind speed (*U*) and power density (*P*). The generalized wind climates are for h=100 m and z_0=0.03 m. The OWA uses default heat fluxes in the WAsP models [19].

3.2. Evaluating seasonal and diurnal cycles in WRF

The time continuous WRF simulation allows for qualitative time-series evaluations of the wind output against data from the 10 measurement masts. As all the masts are situated in relatively flat areas with homogenous land cover, we use the corresponding 3 km square WRF grid cell in which the mast would be situated for the analysis. The validation of the WRF wind output is carried out for wind speeds at 62 m A.G.L.

At WM01, wind speeds are highest in the afternoon and early evening during the austral summer months (Fig. 5). The WRF model captures the shape of the mean seasonal cycle very well with only a small over-simulation (under-simulation) of wind speeds in June and July (August to December). The model also captures the shape of the diurnal cycle of wind speed extremely well with a slight phase error; the maximum in wind speed is at 1600 in WRF while at 1800 in the observations.

Highest wind speeds at WM05 are in the austral spring and summer during the early afternoon to early evening (Fig. 6). The model generally under-simulates the wind speed in summer and over-simulates wind speed in winter but simulates the shape and magnitudes of the diurnal cycle very well.

Only one continuous year of complete data was available from WM10, namely 2011. Highest wind speeds were generally measured in the afternoon with a maximum in June (Fig. 7). The model captures the shape of seasonal cycle (in this year) although it over-simulates autumn and winter wind speeds and under-simulates spring and summer wind speeds. The model captures the shape of the diurnal cycle, but the early morning peak in wind speeds simulated by WRF (largely a function of over-simulating June early morning wind speeds) in not observed.

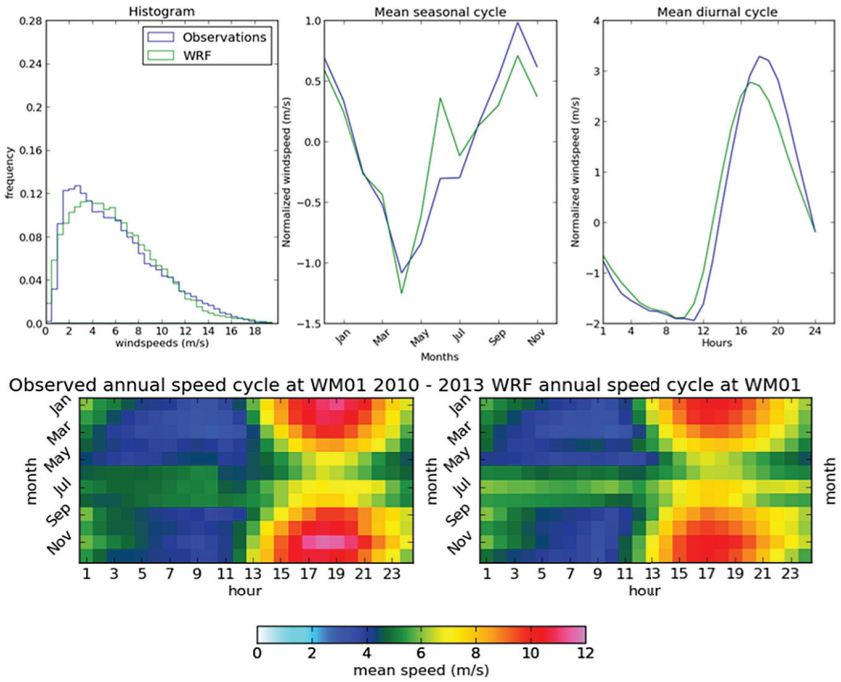

Fig. 5. Comparison of the wind speed characteristics between the WRF simulation and measurement sites at WM01 at 62 m AGL. Wind speed distribution (top left), mean seasonal cycle (top center) and mean diurnal cycle (top right) in the mast measurements (blue) and in the WRF model simulations (green). In the bottom row is a heat diagram of mean wind speed (ms^{-1}) as a function of the time of the day (x-axis) and the month of the year (y-axis) for the mast observations (bottom left) and the WRF simulations (bottom right).

4. Summary and Discussion

Two numerical wind atlases have been created and verified over a region of South Africa, one based on a statistical-dynamical method using the KAMM mesoscale model and the other a fully dynamical method using the WRF mesoscale model. Compared against an observed wind atlas developed at 10 measurement sites, the KAMM-derived NWA underestimates and WRF-derived NWA overestimates the generalized mean wind speeds. However, the WRF mean error is much lower than the KAMM mean error. The WRF NWA has smaller wind speed biases at 8 measurement sites and a lower mean error and mean absolute error across the 10 stations. The wind climate in terms of speed and direction is generally better reproduced in the WRF NWA although at some sites there was little difference between the two NWAs and the OWA. The more simplistic initialization of the large-scale flow in the KAMM modeling, is probably responsible for most of the discrepancies. The WRF model, being time synchronous and receiving boundary conditions every 6 hours from the driving reanalysis, is better suited to resolve complex wind processes and to produce a more realistic regional wind climate.

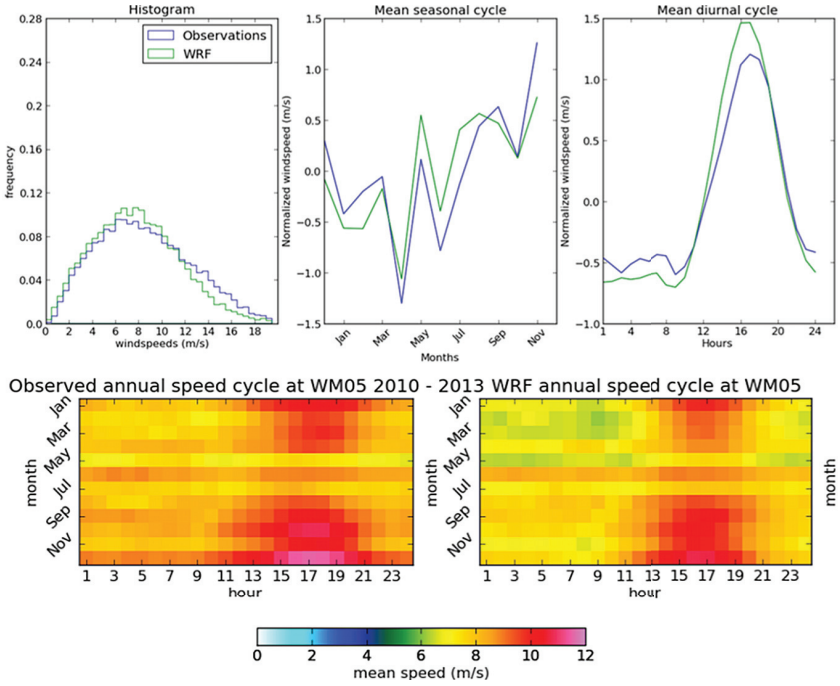

Fig. 6. As for Fig. 5 except at WM05.

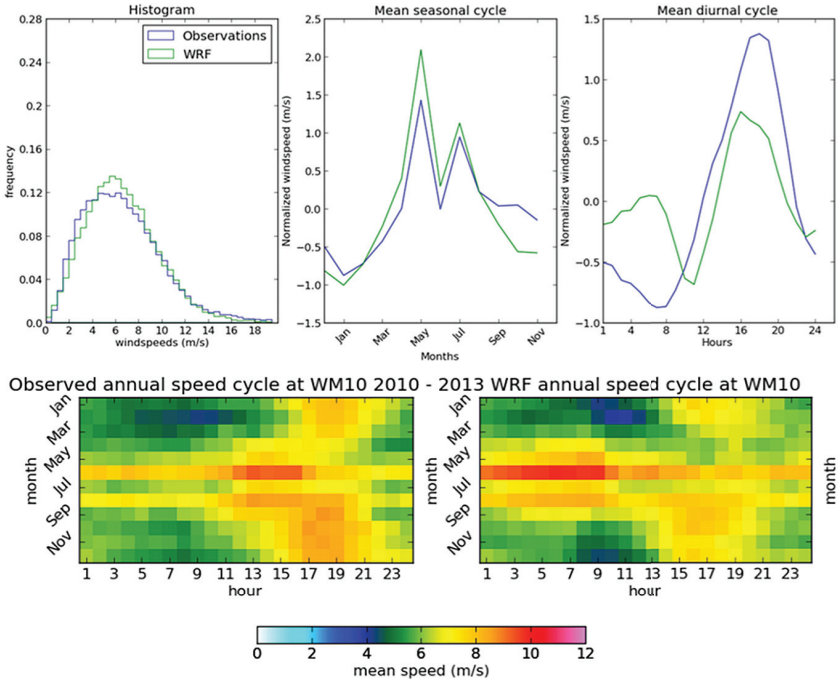

Fig. 7. As for Fig. 5 except at WM10.

The WRF method, however, is computationally expensive to run and poses challenges in post processing of the large data volume produced. Furthermore, uncertainties within this modelling framework that arise from the reanalysis data used to force the model, the model configuration, the representativeness of the period used in constructing the atlas and errors in the generalization method still need to be considered.

Despite these considerations, it has been demonstrated that the WRF-derived NWA has much lower biases than the KAMM-derived atlas. This is especially relevant where power derived from wind is a function of the cube of the wind speed. A fully dynamical wind atlas method provides a superior assessment of wind resource in regions where measurements are sparse and provides more accurate wind climate information for decision-making processes.

Acknowledgements

This paper is based on results and reports of the Wind Atlas for South Africa (WASA) project, which is an initiative of the South African Department of Energy co-funded by the Royal Danish Embassy and UNDP-GEF. The WASA project is coordinated by South African National Energy Development Institute (SANEDI) and implemented by the following partners: Council for Scientific and Industrial Research (CSIR), University of Cape Town (UCT), South African Weather Service (SAWS) and DTU Wind Energy.

References

[1] Landberg L, Myllerup L, Rathmann O, Petersen EL, Jørgensen BH, Badger J, Mortensen NG. Wind resource estimation—an overview. Wind Energy 2003;6:261-271.

[2] Adrian G, Fiedler F. Simulation of unstationary wind and temperature fields over complex terrain and comparison with observations. Beitr Phys Atmosph 1991;64:27–48.

[3] Badger J, Frank H, Hahmann AN, Giebel G. Wind-Climate Estimation Based on Mesoscale and Microscale Modeling: Statistical-Dynamical Downscaling for Wind Energy Applications. J Appl Meteorol Climatol 2014;53:1901–1919.

[4] Frank HP, Landberg L. Modelling the wind climate of Ireland. Boundary-Layer Meteorology 1997;85:359–378.

[5] Frank HP, Landberg L. Numerical simulation of the Irish wind climate and comparison with wind atlas data. In Watson R, editor. Proceedings of EWEC '97. Irish Wind Energy Association: Dublin; 1998. p. 309–312.

[6] Frank HP, Rathmann O, Mortensen NG, Landberg L. The numerical wind atlas – the KAMM/WAsP method. Risø-R-1252(EN). Risø National Laboratory, Roskilde; 2001.

[7] Troen I, EL Petersen. European Wind Atlas. Risø National Laboratory, Roskilde, Denmark; 1989.

[8] Mortensen NG, Hansen JC, Badger J, Jørgensen BH, Hasager CB, Youssef LG, Said US, Moussa AAE-S, Mahmoud MA, Yousef AES, Awad AM, Ahmed MA-ER, Sayed MAM, Korany MH, Tarad MA-EB. Wind atlas for Egypt. Measurements and modelling; 1991-2005. Roskilde: Risø National Laboratory, 2006. 258 p.

[9] Tammelin B. et al. Production of the Finnish wind atlas. Wind Energy 2013;16:19-35.

[10] Skamarock WC, et al. A Description of the Advanced Research WRF Version 3. Tech. Rep. NCAR/TN–475+STR. National Center for Atmospheric Research, Boulder; 2008.

[11] Hahmann, AN, Vincent, CL, Peña, A, Lange, J & Hasager, CB Wind climate estimation using WRF model output: method and model sensitivities over the sea. International Journal of Climatology 2015;10.1002/joc.4217.

[12] Hahmann, AN, Lennard, C, Badger, J, Vincent, CL, Kelly, MC, Volker, PJH, Argent, B & Refslund, J. Mesoscale modeling for the Wind Atlas of South Africa (WASA) project. DTU Wind Energy. DTU Wind Energy E, no. 0050 (updated); 2015. http://orbit.dtu.dk/services/downloadRegister/107110172/DTU_Wind_Energy_E_0050.pdf.

[13] Mortensen NG, Hansen JC, Kelly MC, Prinsloo E, Mabille E, Szewczuk S. Wind Atlas for South Africa (WASA) Station and Site Description Report. Roskilde: DTU Wind Energy; 2014. 70 p. (DTU Wind Energy E; No. 0071(EN)).

[14] Mortensen NG, Hansen JC, Kelly MC, Szewczuk S, Mabille E, Prinsloo E. Wind Atlas for South Africa (WASA) Observational wind atlas for 10 met. stations in Northern, Western and Eastern Cape provinces. DTU Wind Energy; 2014. 64 p. (DTU Wind Energy E; No. 0072(EN)).

[15] Frey-Buness F, Heimann D, Sausen R. A statistical-dynamical downscaling procedure for global climate simulations. Theor Appl Climatol 1995;50:117–131.

[16] Kanamitsu M, Ebisuzaki W, Woollen J, Yang SK, Hnilo JJ, Fiorino M, Potter GL. NCEP-DOE AMIP-II Reanalysis (R-2). Bulletin of the American Meteorological Society 2002;1631-1643.

[17] Dee DP, et al. The ERA-Interim reanalysis: configuration and performance of the data assimilation system. Q J R Meteorolog Soc 2011;137:553–597.

[18] Gemmill W, Katz B, Li X. Daily real-time global sea surface temperature – high resolution analysis at NOAA/NCEP. Oce note nr. 260, 39 pp, NOAA/NWS/NCEP/MMAB; 2007.

[19] Mortensen NG, Heathfield DN, Rathmann O, Nielsen M. Wind Atlas Analysis and Application Program: WAsP 11 Help Facility. Department of Wind Energy, Technical University of Denmark, Roskilde, Denmark. 366 topics; 2014.